Rapid Simulation and Phase Distortion Evaluation of Thermal Blooming Effect in Internal Laser Propagation Channels

Wu Dong-yu[1,2], Li Xiang[1,3*], Li Jia-sheng[3], Gao Liang[1,3],

Song Yan-song[1,3], Wang Si[3], Dong Ke-yan[1,3]

1 Institute of Space Ophotoelectronics Technology, Changchun University of Science and Technology, Changchun 130022, China

2 School of Mechanical and Electrical Engineering, Changchun University of Science and Technology, Changchun 130022, Jilin, China;

3 School of OptoElectronic Engineering, Changchun University of Science and Technology, Changchun 130022, Jilin, China;

* Corresponding Author, E-mail: abelfeel@163.com

Abstract: During the propagation of high-power lasers within internal channels, the laser beam heats the propagation medium, causing the thermal blooming effect that degrades the beam quality at the output. The intricate configuration of the optical path within the internal channel necessitates complex and time-consuming efforts to assess the impact of thermal blooming effect on the optical path. To meet the engineering need for rapid evaluation of thermal blooming effect in optical paths, this study proposes a rapid simulation method for the thermal blooming effect in internal optical paths based on the finite element method. This method discretizes the fluid region into infinitesimal elements and employs finite element analysis for flow field analysis. A simplified analytical model of the flow field region in complex internal channels is established, and regions with similar thermal blooming effect are divided within this model.Based on the calculated optical path differences within these regions, numerical simulations of phase distortion caused by thermal blooming were conducted.The calculated result were compared with those obtained using existing methods. The findings reveal that for complex optical paths, the discrepancy between the two approaches is less than 3.6%, with similar phase distortion patterns observed. For L-type units,this method and existing methods identify the same primary factors influencing aberrations and exhibited consistent trends in their variation. This method was used to analyze the impact of thermal blooming effect in a straight channel under different gravity directions. The results show that phase distortion varies with changes in the direction of gravity, and the magnitude of the phase difference is strongly correlated with the component of gravity perpendicular to the optical axis. Compared to existing methods, this approach offers greater flexibility, obviates the need for complex custom analysis programming.The analytical

results of this method enable a rapid assessment of the thermal blooming effect in optical paths within the internal channel. This is especially useful during the engineering design phase. These results also provide crucial references for developing strategies to suppress thermal blooming effect.

激光内通道热晕效应的快速模拟与相位畸变评估

吴东宇 [1,2]，李响 [1,3*]，李家晟 [3]，高亮 [1,3]，宋延嵩 [1,3]，王思 [3]，董科研 [1,3]

1. 长春理工大学 空间光电技术研究所，吉林 长春 130022；
2. 长春理工大学 机电工程学院，吉林 长春 130022；
3. 长春理工大学 光电工程学院，吉林 长春 130022；

摘要 高功率激光在内通道传播过程中，光束会在导光路径中加热传播介质产生热晕现象，影响高能激光设备出光口处光束质量；由于内通道中光路排布复杂，因此对导光路径上热晕影响的评估往往需要复杂的工作和较长的时间。为适应工程中对导光路径热晕效应快速评估的需要，本文提出一种基于有限元法的内光路热晕效应快速模拟方法。该方法对流体区域进行微元划分，利用有限元分析方法进行流场分析；对复杂内通道的流场区域建立简化分析模型，在简化模型中划分等晕区域；根据各等晕区域内光程差计算结果，完成热晕效应导致的相位畸变的数值模拟计算。将计算结果与现有方法计算结果对比，结果显示：对于复杂光路，该方法计算结果与现有方法计算结果偏差小于 3.6%，相位畸变形式相近；对于 L 型单元，该方法计算结果与现有方法计算结果得到的主要像差影响因素和变化规律相同。利用该方法完成对直管道不同重力作用方向下的热晕影响分析，结果显示，相位畸变随重力方向变化而变化，相位变化的大小与重力在垂直于光轴方向的分量大小有很强的相关性。该方法相较于现有方法灵活性高、无需进行复杂自编分析程序调试。该方法的分析结果在工程设计阶段能够快速评估内通道导光路径中热晕效应，为确定热晕抑制方法提供重要参考。

关键词 高能激光；热晕效应；光束相位；数值模拟；热耦合效应；光束控制系统

1 Introduction

With over half a century of development, laser technology has matured significantly[1]. High-power lasers, characterized by their high pointing accuracy and long propagation distances, are capable of delivering energy swiftly and precisely to distant targets[2,3]. However, during the propagation of high-power lasers , the small beam diameter and high energy density often cause localized heating of the propagation medium, leading to thermal blooming[4,5]. This phenomenon results in beam phase distortion, significantly degrading the output beam quality and the far-field beam energy concentration of laser systems[6].Xiangyizheng Wu[7]analyzed the deterioration of the beam's β factor in a closed region with different gas media under the effect of airflow alone using simulation analysis. By comparing the analysis results with experimental data, it was shown that both exhibited the same variation trend, with the difference between the two being an order of magnitude smaller than the actual result.Therefore, it is crucial to suppress the thermal blooming effect during the

propagation of high-power lasers in internal channels. Researchers have explored and confirmed the positive effects of introducing gas curtains or low-absorption gases in internal channels to suppress the thermal blooming[8, 9].Nevertheless, in practical engineering, it remains essential to accurately and rapidly assess the impact of the thermal blooming effect to provide data support for selecting appropriate thermal blooming suppression strategies.

Regarding the numerical simulation of the thermal blooming effect in high-power lasers, researchers have already achieved numerous significant results. In the 1970s, Bradley and Herrmann[10] at Lincoln Laboratory developed a computer simulation program for laser propagation in absorbing media, which effectively analyzed steady-state thermal blooming effects but was limited in analyzing transient thermal effects of high-power lasers. In 2011, Sun Yunqiang[11] from the National University of Defense Technology utilized the custom subroutine function of FLUENT to couple the optical field and flow field. By dividing the propagation area into multiple sub-regions for iterative solving, this method effectively determined the optical field at the laser system's exit. In 2017, Zhu Fuyin[12] from the Institute of Optics and Electronics, Chinese Academy of Sciences, employed a similar approach to analyze the impact of thermal blooming on phase differences at the exit under both non-blowing and blowing conditions, and experimentally validated the method's accuracy. However, these methods require complex secondary development of simulation software and separate meshing of the optical field for calculations, making them unsuitable for rapid assessment needs during the early stages of engineering design. In 2022, Hu Peng [13] and colleagues from the Beijing Institute of Applied Physics and Computational Mathematics studied the effects of various factors on thermal effects in horizontal enclosed light-conducting pipes and introduced internal optical path analysis software. This software can perform the thermal blooming simulation task but requires substantial computational resources and the ability to rapidly assess the thermal blooming effect in complex three-dimensional propagation paths can still be improved. In 2024, Rui Zhou[14] introduced a method for analyzing thermal blooming effect using grid-wise integration approach in their study. This approach, which leverages finite element analysis, significantly simplifies the process of analyzing thermal blooming. However, grid-wise integration approach itself may encounter mesh mismatch issues in complex regions.Therefore, designing a practical and straightforward analysis model that meets the needs for rapid assessment of high-power laser gas the thermal blooming effect in engineering remains a crucial issue in the current engineering field.

To provide a reference solution to the aforementioned issues, an equivalent analysis method for thermal blooming effect in the optical path is proposed. This method utilizes finite element analysis for flow field calculations. By constructing an equivalent analysis model and dividing the regions with identical thermal blooming effect, the impact of thermal blooming effect in the internal channel on the beam phase can be determined. Compared to existing methods, this model offers a simpler equivalent process, a more flexible data handling method, and eliminates the need for complex software development, making it highly practical and accurate. The analytical results of this method provide references for engineering design.

2 Theoretical Model

The thermal blooming effect in the internal channel light path occurs when some of the gas in the propagation path absorbs laser energy upon irradiation. The irradiated gas undergoes a localized temperature increase, altering its density. In the absence of external lateral wind interference within the internal channel, the gas flows under the influence of gravity once its density changes. Furthermore, the non-uniform density distribution leads to a non-uniform refractive index during beam propagation, resulting in a phase difference[15].

Based on an analysis of the mechanisms behind thermal blooming, the process includes two main components: the analysis of density distribution resulting from the interaction between the fluid and high-power laser, and the optical path difference analysis as the beam traverses a non-uniform medium.

2.1 Solving for Density Distribution

The density of a gas is influenced by pressure and temperature, and their relationship is described by the ideal gas law, expressed as follows:

$$PV = nRT \qquad (1)$$

Where P represents the gas pressure; V is the gas volume; T denotes the gas temperature; n is the amount of substance; R is the molar gas constant, typically R =8.31 J/(mol·K).

The gas density within the infinitesimal element is:

$$\rho = \frac{m}{V} = \frac{M \cdot n}{V} = M \cdot \frac{P}{RT} \qquad (2)$$

where ρ is the gas density, m is the infinitesimal element mass, M is the molar mass.

The gas flow inside the closed pipe is driven by natural convection, caused by non-uniform density distribution and gravity. Due to the relatively small temperature rise, the impact of density changes on volume variation is negligible.Therefore, the model is simplified to an incompressible laminar flow model[16,17]. The laser irradiation energy is considered as a heat source in the spot area. Under these conditions, the density distribution in the airflow can be determined using the conservation equations of mass, momentum, and energy[18].

The mass conservation equation states that the mass entering an infinitesimal element per unit time is equal to the increase in mass within that infinitesimal element:

$$\frac{\partial \rho}{\partial t} + \nabla(\rho U) = 0 \qquad (3)$$

Where U is the velocity vector; in incompressible flow, $\nabla(\rho U) = 0$

The momentum conservation equation states that the rate of change of momentum is equal to the net force acting on the infinitesimal volume element:

$$\frac{\partial U}{\partial t} + U \cdot \nabla U = -\frac{1}{\rho}\nabla p + G \qquad (4)$$

Where G is the gravitational force.

The energy conservation equation states that the increase in energy of an infinitesimal volume element is equal to the work done on it by the energy entering the element.

$$\frac{\partial(\rho T)}{\partial t} + \nabla \cdot (\rho U T) = \nabla \cdot (\frac{k}{\rho c}\nabla T) + \frac{Q}{\rho c} \qquad (5)$$

Where k is the thermal conductivity of the gas; c is the specific heat capacity of the gas; Q is the heat entering the infinitesimal element.

In the analysis of the heating effect of laser on gas, the energy Q entering the gas infinitesimal volume element is related to the gas absorption rate and the laser intensity distribution.The absorbed energy $Q(x,y,z)$ of the infinitesimal element at point (x,y,z) in space can be expressed as:

$$Q(x,y,z)=t \cdot P(x,y,z)=t \cdot \eta \cdot I(x,y,z) \quad （6）$$

Where $P（x,y,z）$ is the power of the energy absorbed by the infinitesimal volume element at the point (x,y,z) in space; t is the duration; η is the absorption rate of the gas for the specific wavelength of the laser; $I（x,y,z）$ is the intensity distribution at that point.

Using the finite element analysis method, the medium region is divided into multiple infinitesimal elements. By applying the aforementioned equations, the temperature change of the gas within each infinitesimal volume element after heating can be determined. Consequently, the density change within each infinitesimal volume element can be calculated.

2.2 Equivalent Model for Bent Light Path

After determining the density within each infinitesimal element, it is necessary to evaluate the specific impact of thermal blooming on beam quality deterioration through the beam's phase difference. For the analysis of thermal blooming effect in complex internal channels, this study employs an equivalent substitution method to simplify the calculation process. The equivalent modeling procedure is as follows:

Assume the L-type light path within a spatial coordinate system, containing an equivalent mirror, incident light, and reflected light. In the L-type light path, the spatial coordinates of the center of any infinitesimal volume element are (x_i,y_i,z_i), the gas density within this infinitesimal volume element is ρ_h, and the coordinates of any three points on the equivalent plane of the mirror are $P_1(x_1,y_1,z_1)$, $P_2(x_2,y_2,z_2)$, and $P_3(x_3,y_3,z_3)$. The positions are illustrated in Fig. 1.
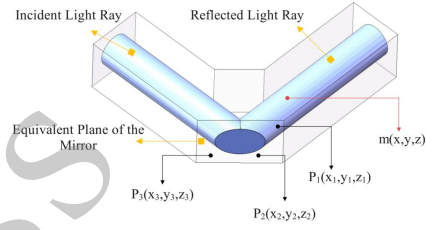

Fig. 1 Schematic diagram of point positions within the L-type light-passing region

The two vectors $\vec{v}_1$ and $\vec{v}_2$ on the equivalent plane of the mirror can be expressed as:

$$\begin{cases} \vec{v}_1=P_1-P_2=(x_1-x_2,y_1-y_2,z_1-z_2) \\ \vec{v}_2=P_3-P_2=(x_3-x_2,y_3-y_2,z_3-z_2) \end{cases} \quad （7）$$

The normal vector $\vec{n}$ of the equivalent plane of the mirror is expressed as:

$$\vec{n} = \vec{v}_1 \times \vec{v}_2 \quad （8）$$

The coordinates of the selected point are $h(x,y,z)$.The vector from $h(x,y,z)$ to $P_1(x_1,y_1,z_1)$,which can be determined based on the coordinates of the two points, is denoted as $\vec{m}=(x-x_1,y-y_1,z-z_1)$. According

to the spatial relationship of vectors, the point $h'(x', y', z')$, which is the mirror image of the $h'(x', y', z')$ selected point $h(x, y, z)$ after reflection by the equivalent plane of the mirror, can be calculated. The relationship between them is as follows:

$$(x', y', z') = (x, y, z) - \frac{2(\vec{m} \cdot \vec{n})}{\vec{n} \cdot \vec{n}} \vec{n} \quad (9)$$

After the equivalent mirroring, the density at the equivalent point h' of h is $\rho_{h'} = \rho_h$. The original L-type light path can be equivalently represented as a straight light path, as shown in Fig. 2
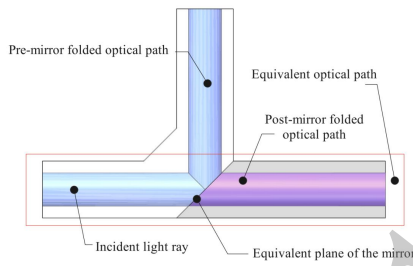

Fig. 2 Schematic diagram of optical path equivalence

2.3 Phase Distortion Calculation

The perturbation method is the simplest and most efficient approach commonly used for calculating the thermal blooming effect. This method treats the distortion caused by thermal blooming as a perturbation term added to the original undistorted beam. As a method of geometric optics method, it ignores the effect of diffraction[19].Given the short propagation distance and minimal external influences in the internal light path. This method as the theoretical basis for evaluating the phase distortion induced by thermal blooming effect in the internal light path in this study.

Based on the equivalent straight light path, the equivalent phase distribution of the beam affected by the thermal blooming effect

as it traverses the system is calculated.The coordinate system is oriented such that the Z-axis aligns with the direction of light propagation. In the cross-section perpendicular to the light propagation direction, the area is divided into m units along both the X-axis and Y-axis, creating m^2 regions within the equivalent flow field. When these regions are sufficiently small, the thermal blooming effect is assumed to be uniformly distributed within each region, referred to as a region with identical thermal blooming effect. The side lengths of each region with identical thermal blooming effect in the X-axis and Y-axis directions are Δx and Δy, respectively, while the unit thickness corresponds to the light propagation distance. This subdivision process is depicted in Fig.3.
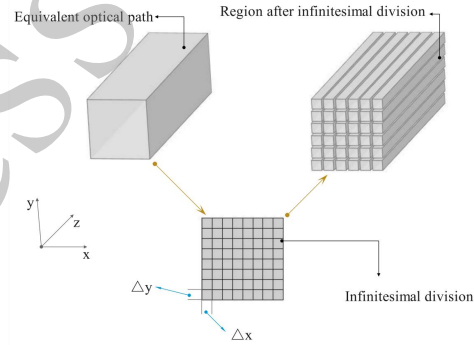

Fig. 3 Schematic diagram of computational unit division

Each region with identical thermal blooming effects contains H infinitesimal volume element . The average density ρ_{average} within each region with identical thermal blooming effect is calculated as follows:

$$\rho_{\text{average}} = \frac{\sum_{i=1}^{H} \rho_i}{H} \quad (10)$$

where ρ_i is the density of an infinitesimal volume element within the

region with identical thermal blooming effect.

According to the Gladstone-Dale relation [7,20] the average refractive index n_{average} within each region with identical thermal blooming effect can be calculated as follows:

$$n_{\text{average}} = K \cdot \rho_{\text{average}} + 1 \qquad (11)$$

$$K \approx (n_s - 1)(1 + \frac{\alpha T}{P}) \qquad (12)$$

where K is the Gladstone-Dale constant. $\alpha = 1/273.15\text{K}$. The refractive index n_s can be obtained through measurements under standard conditions (T = 293.15 K, P = 1 atm).

The phase difference $\Delta\varphi_i$ induced by the beam passing through the regions with identical thermal blooming effect is expressed as:

$$\Delta\varphi_i = \frac{2\pi}{\lambda} OPD = \frac{2\pi}{\lambda}(n_{\text{average}} - n_s)L \qquad (13)$$

where OPD is the optical path difference, L is the beam propagation distance, and λ is the wavelength of the beam, n_s is the refractive index of the gas under standard conditions.

After determining the phase difference for each region with identical thermal blooming effect, the spatial position distribution of these regions can be used to obtain the equivalent analysis results of the phase difference distribution caused by thermal blooming effect during beam propagation.

3 Simulation Model

The laser propagation channel analyzed in this study is a serpentine path, with the simplified model of the optical path shown in Fig.4. The optical path includes three 45° mirrors and two 22.5° mirrors. Gravity acts in the negative Y-axis direction on the medium within the optical path.Due to the influence of gravity, the light path can be divided into two horizontal light-transmitting regions and two vertical light-transmitting regions.
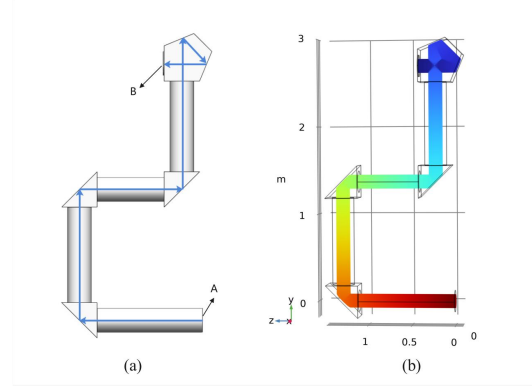

Fig. 4 Analysis model of light propagation channel: (a)Simplified model of light propagation channel; (b)Optical path model

The beam is incident perpendicular to surface A and exits perpendicular to surface B after five reflections. The beam diameter is 150 mm, and the light propagation channel diameter is 250 mm. The type of beam used in this study is a Gaussian flat-top beam, with the cross-sectional intensity distribution given by the following expression:

$$I(x,y) = I_o \sum_{n=0}^{N} \frac{1}{n!}\left(\frac{x^2 + y^2}{w_{oN}^2}\right)^n \exp\left(-\frac{x^2 + y^2}{w_{oN}^2}\right) \qquad (14)$$

Where, $w_{0N} = w_0/\sqrt{N+1}$, N is the order of expansion, w_0 is the beam waist radius of the flat-top beam spot, and I_o is the peak light intensity.

In the study, the wavelength of the light beam is 1064 nm. The distribution of the gas absorption power in the cross-section, obtained by multiplying the gas absorption coefficient η with the light intensity I , is

shown in Fig.5. The power density at the flat-top region is 400 W/m^3. The beam propagation time in this study is 3 seconds.
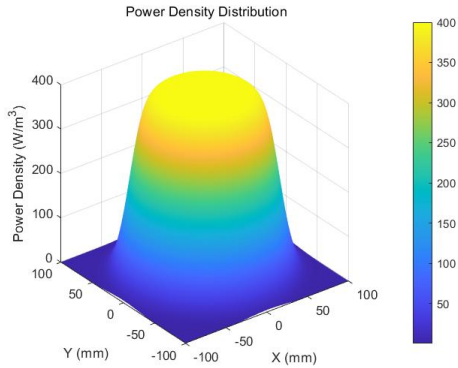

Fig.5 Energy distribution diagram of the beam used in the study

In this study, the finite element method (FEM) was employed for flow field calculations. COMSOL Multiphysics was used to discretize and analyze the flow field in detail.

After simplifying the flow field region, the structure becomes straightforward, and the flow field mesh is divided using a structured grid.The structured mesh can effectively enhance the speed of data storage and access.The boundary regions, including the fluid area in contact with the pipe wall and the lens, exhibited significant variations in medium properties.Therefore, eight layers of boundary layer mesh were added, with each layer having a thickness of D/85, where D represents the diameter of the light propagation region. Given the substantial temperature variations in the irradiated area at the center of the light propagation path, this region's mesh was refined to improve the accuracy of medium temperature rise calculations. The overall mesh element growth rate was maintained below 1.1.High-order elements are used in the calculations to improve the accuracy of the sampled node data in representing the overall simulation data.The total number of mesh elements is 1,851,075. The mesh element division model is shown in Fig.6.
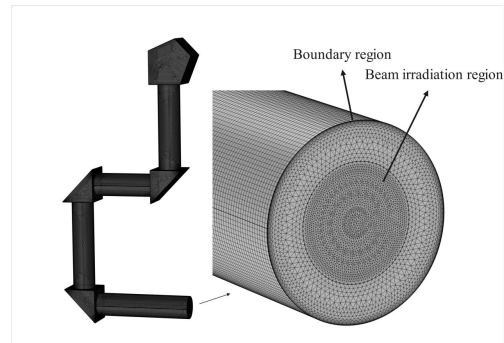

Fig. 6 Meshing model of the fluid region

Due to the short laser irradiation time, the air density near the tube wall in the flow field changes minimally during laser loading, and there is almost no gas flow, the contact regions between medium and the pipe wall are set as no-slip boundaries. Since the medium in the light propagation path is influenced only by gravity, the gas flow speed is slow, the flow field simulation uses an incompressible flow.Considering that the gas under study is at normal temperature and pressure with low viscosity, the $k-\varepsilon$ model is employed for simulation. Given that the analyzed environment is static, with no air movement in the flow field, the flow velocities at surfaces A and B of the simplified light propagation pipeline model are set to 0 m/s.

In this study, the propagation medium used is dry air at standard atmospheric pressure. The material properties are shown in Tab.1.

Tab. 1 Medium Parameters

Parameter Type	Parameter Value
Density/（kg/m^3）	1.17
Specific Heat at Constant Pressure/ (J/kg·K)	1006
Specific Heat at Constant Volume/ (J/kg·K)	718
Viscosity/(10^{-5}Pa·s)	1.81
Thermal Conductivity/(W/(m·K)	0.0257

The initial temperature of the environment is set to 300 K. After 3 seconds

of light propagation, the temperature distribution at the center cross-section under no-wind condition is shown in Fig.7. The temperature rise occurs in the regions where the light paths intersect, with a maximum temperature increase of 2.163 K. In areas without overlapping light path, the temperature rise is approximately 1 K.
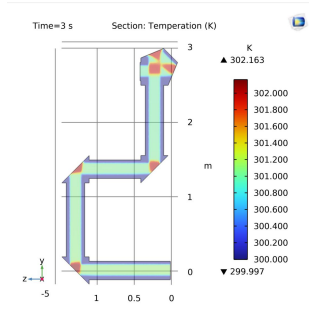

Fig. 7 Temperature distribution after 3 seconds of light propagation

The density variation, which directly influences the refractive index.The density is initially set to 1.17 kg/m³ for the propagation medium within the optical path,as shown in Fig.8(a). The density values at each node after 3 seconds of light propagation, calculated using finite element analysis. The density distribution on the central cross-section is shown in Fig.8(b). The density significantly decreases in the light path coverage area due to the temperature effect, with the non-overlapping region of the light path experiencing a density reduction of approximately 0.005 kg/m³ and the overlapping region experiencing a reduction of 0.01 kg/m³. Additionally, it is observed that under the influence of gravity, the propagation medium with lower density exhibits a clear buoyancy effect.

The node density distribution obtained from the finite element analysis software is extracted and shown in Fig.8(c). Based on Equation (9), the equivalent model of the refracted light path was established, as shown in Fig.8(d).
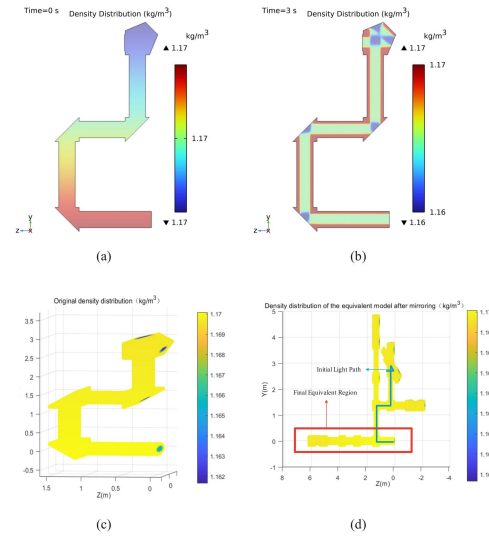

Fig. 8 Density equivalent model calculation process diagram :(a) Initial density distribution; (b) Density distribution after 3 seconds of light propagation;(c) Density nodes of the original model; (d) Density nodes of the equivalent mode

4. Analysis Result Validation

4.1 Optical path analysis validation

In the equivalent light propagation region model, the division of regions with identical thermal blooming effect and the calculation of the average density and optical path difference within these regions were completed.

The specific process is as follows: regions with identical thermal blooming effect are divided in the cross-section perpendicular to the light propagation direction, with m axial units along both the X-axis and Y-axis. As the number of axial units m increases, the calculation accuracy improves, but the computation time also increases. The relationships between the number of axial units m and the calculated phase difference, as well as between the number of axial units m and the computation time, are analyzed. The results are shown in Fig.9. As the number of axial units varies from 64 to 1064, the computation time exhibits a clear upward trend. When the number of axial units exceeds

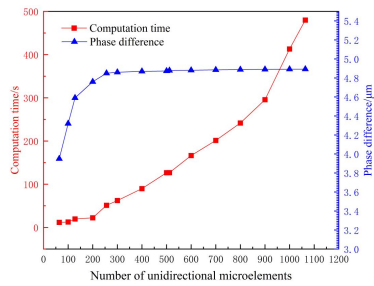256, the calculation results stabilize, and the data show significant convergence.

Fig.9 Calculation time and results with different numbers of unidirectional micro-elements

Fig.9 shows the relationship between computation time and results with different numbers of axial micro-elements. In the final analysis, the number of axial elements along the X-axis and Y-axis was set to $m = 256$.

Based on Equation (11) and equation (13), the phase distribution at the output port is obtained, as shown in Fig.10. From the phase distribution image, it can be observed that under the influence of gravity, the calculation result of the equivalent model proposed in this study exhibit a phase distribution with distinct double-fisheye characteristics. Due to the energy distribution characteristics，at the cross-section of the flat-top beam, the phase variation rapidly decreases at the edges of the beam. After 3 seconds of laser irradiationthe，phase distortion of 4.7568 μm and a phase difference peak-to-valley (PV) of 2.9504 μm.
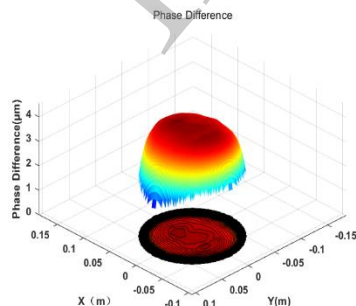

Fig.10 Computed beam phase difference distribution

Using a self-developed program validated by experiments[12], the simplified model of the same light propagation path was analyzed.After analyzing the thermal blooming effect following 3 seconds of laser irradiation in a no-wind environment,The results indicate a phase distortion of 4.9364 μm and a phase difference PV of 3.1949 μm.

By comparing the calculation results of the two methods, the deviation in phase distortion magnitude is less than 3.6%, and the deviation in phase PV is less than 7.7%.

The obtained normalized beam wavefront aberration is shown in Fig.11.
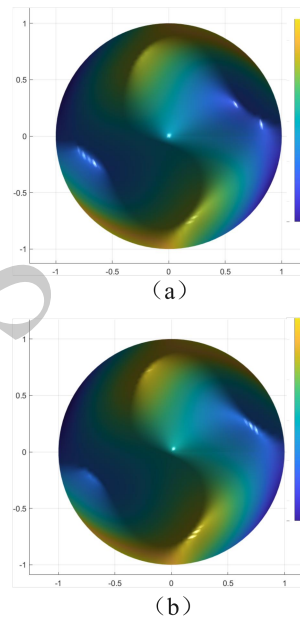

（a）

（b）

Fig.11 Beam wavefront aberration:(a)Wavefront aberration calculated by the model;(b)Wavefront aberration calculated by the self-developed program

The comparison of wavefront aberration clearly demonstrates that the results calculated by the analytical model proposed in this study are highly consistent with those from existing programs.

Zernike polynomials are a set of orthogonal polynomials that can accurately describe wavefront errors and aberrations on a unit circle[21,22]. The phase distortion calculated from the equivalent model and the self-developed program were fitted using Zernike polynomials. Standard Zernike

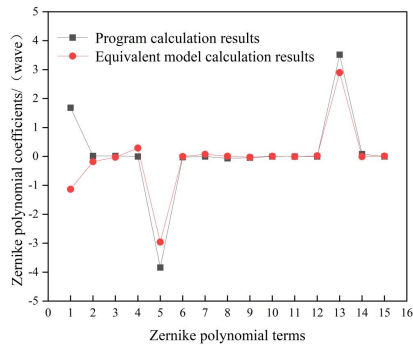polynomials were selected for the fitting process. The comparative fitting results are shown in Fig.12.

Fig.12 Comparison of Zernike polynomials

According to the comparative results in Fig.12, the calculations from the equivalent model and the self-developed program show a high degree of similarity. The differences are mainly reflected in the coefficients of the first, fifth, and thirteenth terms. The first, fifth, and thirteenth terms of the standard Zernike polynomials correspond to the tilt, the defocus, and the spherical aberration, respectively[23].

Except for the first coefficient, which shows a significant difference, the variation trends of the other coefficients are generally consistent. The coefficients that have a substantial impact on phase distortion are the defocus and spherical aberration terms. The first term of the standard Zernike polynomials primarily represents the overall phase shift, which does not affect the actual beam quality.

Since this study uses a method of calculating phase distortion through regions with identical blooming effect for equivalence, the input data for Zernike fitting is smoother compared to the input data from program calculations. As a result, the Zernike coefficients are slightly smaller than the program calculation results. For the fifth term (defocus), the coefficients from the equivalent model and the program calculations are -2.95 λ and -3.84 λ, respectively. For the thirteenth term (spherical aberration), the coefficients are 3.5 λ and 2.9 λ, respectively.

The phase distortion types calculated by both methods are similar. Combined with the comparison results of phase distortion magnitude and PV, the calculation results of this method have a certain reference value.

4.2 L-type unit analysis validation

The L-type unit is a common basic structure in optical paths. Analyzing the thermal blooming effect within L-type units aids in optimizing the overall performance of optical systems. Therefore, in addition to the comprehensive optical path validation mentioned earlier, this study also includes validation of the accuracy of the thermal blooming effect analysis results for L-type units.

The L-type unit used in this study is shown in the Fig.13. The ratio of the beam diameter to the width of the optical path is 3/8. The beam is a Gaussian beam with an absorption power density of 25 W/m³. The light enters from *A*, is reflected, and exits from *B*, with the gravitational direction aligned with the direction of light incidence.
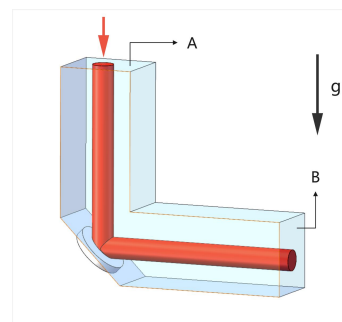

Fig.13 L-type region schematic

During the analysis, the finite element mesh discretization method remains consistent with that described earlier. Helium is used as the propagation medium, with its material properties listed in the Tab.2.

Tab. 2 Physical Properties of Helium

Parameter Type	Parameter Value
Density/ (kg/m³)	1.138
Specific Heat at Constant Pressure/ (J/kg·K)	1040.67
Viscosity/(10^{-5}Pa·s)	1.66
Thermal Conductivity/(W/(m·K)	0.0242

During the analysis, the initial temperature is set to 293.15 K. After 5 seconds of beam irradiation, the temperature distribution at the cross-section is shown in the Fig.14. The temperature rise is highest in the overlapping region of the optical path near the mirror, with gas flow phenomena occurring due to the influence of gravity. The temperature rise in the non-overlapping region of the optical path is approximately 0.4 K.
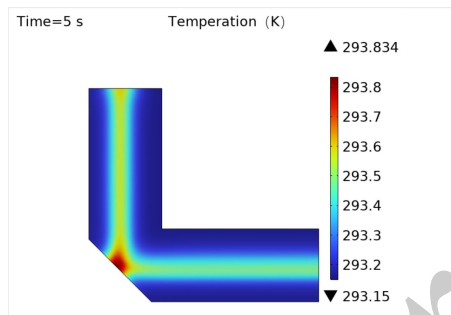

Fig.14 Temperature distribution after 5 seconds

The phase distribution at the output aperture is analyzed using the method described earlier. In this study, standard Zernike polynomials were used for fitting, with the first 15 terms selected for evaluation. The first three Zernike polynomials, which do not affect beam quality, were excluded from the analysis. The resulting Zernike polynomial coefficients at the output aperture are shown in the Fig.15.
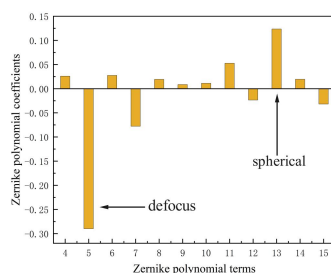

Fig. 15 Zernike coefficients from the 3rd to the 15th terms

In the standard Zernike polynomial, the primary terms affecting wavefront aberrations are the fourth term (astigmatism-A), the fifth term (defocus), the sixth term (astigmatism-B), the eighth term (coma-A), the ninth term (coma-B), and the thirteenth term (spherical). The variation of the main Zernike terms after 5 seconds of beam irradiation is shown in Fig.16.
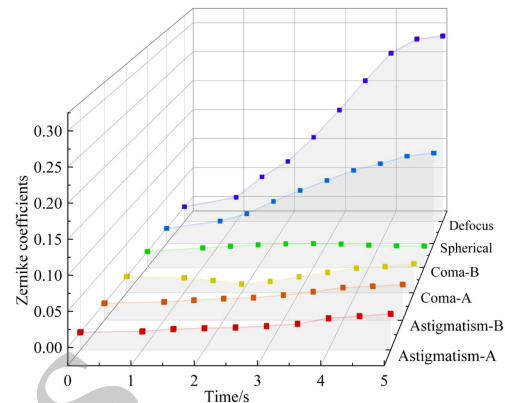

Fig. 16 Variation of the main Zernike terms

It is evident that, after 5 seconds of beam irradiation, the primary aberrations at the output aperture are defocus and spherical aberration.

An analysis of the thermal blooming effect on the same L-type region has also been conducted in the reference[14] The magnitude of aberrations or overall wavefront aberration is commonly assessed using the absolute values of Zernike coefficients, a commom practice in wavefront analysis and optical design. Therefore, the variations in the absolute values of defocus and spherical aberration over 5 seconds of beam irradiation were compared between the results of this study and those reported in the reference, as shown in the Fig.17.
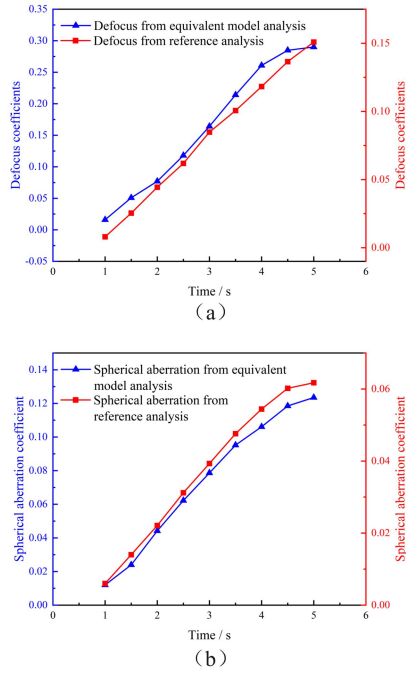
Fig. 17 Defocus and spherical aberration changes over 5 seconds:(a)Defocus;(b)spherical aberration

From the Fig.17, it is evident that, over 5 seconds of beam irradiation, the variation patterns of defocus and spherical aberration from the simplified model proposed in this study are consistent with those in the reference. While specific numerical values differ due to variations in optical path distances, the results are sufficiently accurate to validate the simplified model's effectiveness in assessing thermal blooming effect in the L-type unit.

5 Gravity Effect on Thermal Blooming

Gravity, as an input term in the momentum conservation equation, is a significant factor contributing to gas turbulence within internal channels[24,25]. Different gravity directions result in varying thermal blooming effects. This study employs the aforementioned analytical methods to investigate the thermal blooming effects of gas in a straight circular internal channel under the influence of gravity in different directions.

The straight circular internal channel has a diameter of 250 mm. The distribution of beam energy density, the properties of the propagation medium within the internal channel, and the discretization method for the flow field region are the same as described previously.

The angle between the direction of gravity and the beam direction is denoted as θ, as shown in Fig.18. The range of θ varies from 0° to 180°.The angle θ is taken at observation points of 0°, 30°, 60°, 90°, 120°, 150°, and 180°.The variation process of phase distortion with angle under the influence of thermal blooming effect is documented, as shown in Fig.19.
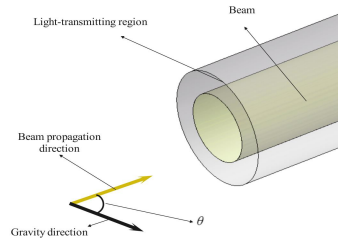

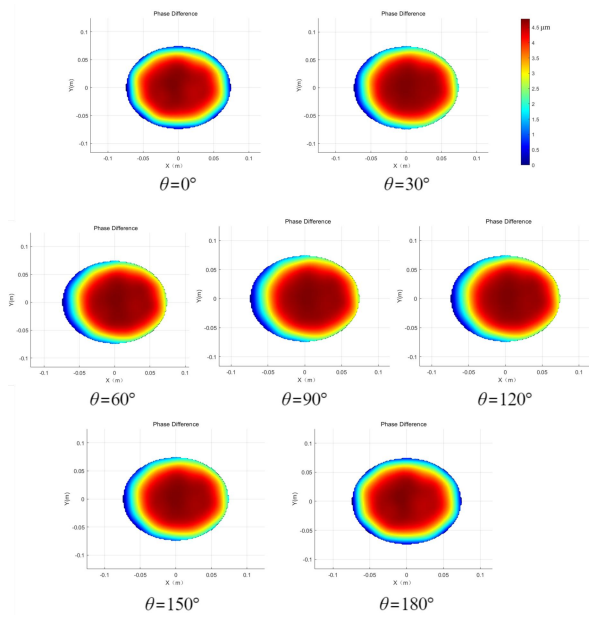Fig. 18 Gravitational force direction diagram

Fig.19 Phase variation distribution under different θ

Based on the analysis results shown in Fig.19, it is evident that under thermal blooming, the phase distortion within the straight circular channel changes with the angle θ. Specifically, when $0°<\theta<90°$, as θ increases, the phase distortion shows a displacement, with larger angle changes resulting in greater displacements. When $90°<\theta<180°$, as θ increases, the displacement of the phase distortion gradually decreases until the phase distortion returns to the central position at $\theta=180°$. The phase distortion distribution exhibits symmetry around $\theta=90°$ under different gravity directions. In the ranges $0°<\theta<60°$ and $120°<\theta<180°$, the displacement of the phase distortion changes significantly with θ. Within these angle ranges, the phase distortion distribution is sensitive to the direction of gravity.

As the angle θ changes, the component of gravity perpendicular to the optical axis undergoes significant variation. The relationship between the gravity component perpendicular to the optical axis and the phase distortion with changing θ is shown in Fig.20. The analysis results show that as the angle θ changes, the magnitude of phase distortion increases from 3.5498 μm at $\theta=0°$ to 4.7568 μm at $\theta=90°$, and then decreases back to 3.5121 μm at $\theta=180°$. The phase distortion trend strongly correlates with the variation trend of the gravity component perpendicular to the optical axis as θ changes. In the ranges $0°<\theta<60°$ and $120°<\theta<180°$, both the phase distortion and the gravity component perpendicular to the optical axis exhibit high rates of change. In the range $60°<\theta<120°$, the phase distortion is more gradual, and the rate of change of the gravity component perpendicular to the optical axis is also lower.
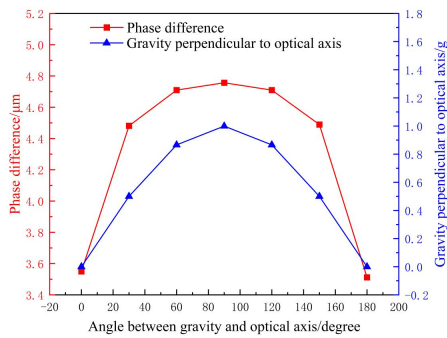
Fig.20 Relationship between gravity component and
phase difference

6 Conclusion

In this work, a rapid simulation model based on the finite element method (FEM) is developed. This model is used to evaluate phase distortion caused by thermal blooming effect during the propagation of high-power lasers within an internal channel.Flow field analysis and micro-element division were first performed using FEM principles. Subsequently, an equivalent model was constructed to calculate the phase distortion induced by thermal blooming effect after 3 seconds of light propagation by a high-power laser with a beam diameter of 150 mm.The results show a distinct 'double fisheye' pattern in the phase distortion distribution, with a phase distortion magnitude of 4.7568 μm and a PV of 2.9604 μm. The primary contributors to phase distortion were identified as the defocus and the spherical aberration. The method was validated by comparing it with existing methods, finding a high degree of similarity in the calculation results between the two approaches.The types of phase distortion were consistent, and the deviation in phase distortion magnitude was less than 3.6%. For L-type units, both methods identified the same primary factors influencing aberrations and exhibited consistent trends in their variation.Additionally, this model was used to evaluate the impact of thermal blooming under different gravity directions. The results show a strong correlation between the magnitude of phase distortion and the component of gravity perpendicular to the optical axis. As the perpendicular component of gravity increases, the phase distortion exhibits centroid shift,with its magnitude increasing from 3.5498 μm to 4.7568 μm, and then decreasing back to 3.5121 μm.This model eliminates the need for developing and debugging complex analysis code, offering significant versatility and flexibility. It is particularly valuable in the early stages of engineering design for the rapid assessment of thermal blooming effect caused by laser propagation in light-propagation paths and for selecting appropriate control strategies.

References：

[1]　任国光,黄裕年.战术高能激光武器的发展和未来[J].激光与红外,2002,32(4):211-217.

　　　REN G G,HUANG Y N.The present status and future of the tactical laser weapons[J].*Laser ＆ Infrared,* 2002,32(4):211-217.(in Chinese)

[2]　王瑞凤,张彦朴,许志艳.激光技术军事应用的现状及发展趋势[J]. 红外与激光工程,2007,36(s)：308-311.

　　　WANG R F,ZHANG Y P,XU Z Y.Present situation and developing trend of application of laser technique to military[J].*Infrared and Laser Engineering,*2007,36(s)：308-311.(in Chinese)

[3]　任国光. 高能激光武器的现状与发展趋势[J].激光与光子学进展,2008,45(9):62-69.

REN G G.Current situation and development trend of high energy laser weapon[J].*Laser & Opto-electronics Progress*,2008,45(9):62-69.(in Chinese)

[4] YUQIU ZHANG,XIAOLING JI,XIAOQING LI,et al.Thermal blooming effect of laser beams propagating through seawater[J].*Optics Express,*2017,25(6):5861-5875.

[5] 张建辉，史春鹏.强激光内光路传输的热晕效应实验研究[J].光电技术应用,2020,35(3):45-49

ZHANG J H,SHI C P,Experimental research on thermal blooming effects of high energy laser internal optical transmission[J].Electro-optic technology application,2020,35(3):45-49.

[6] 金刚，刘顺发，李树民，等.激光热效应对光束控制系统发射光束质量的影响[J].中国激光,2002,29(10):895-899.

JIN G,LIU S F,LI S M,*et al.*Laser thermal effects in beam control system on the emitted laser quality[J].*Chinese Journal of Lasers*,2002,29(10):895-899.(in Chinese).

[7] Xiangyizheng Wu,Jian Xu,Keling Gong,*et al*.Theoretical and experimental studies on high-power laser-induced thermal blooming effect in chamber with different gases[J].*Chin Phys B*,2022,21:086105(1)-086105(6);

[8] McClellan C, Munn M. W, Norris H,etal. Optical effects of gas flow through an optical train: an experimental determination [J]. *Applied Optics*, 1979,18(23): 3984~3989.

[9] Albertine J, R,Sadegn Siahatgar and Bennett H. E. High-power beam control: results to date and relevance to power beaming[C]. *Proc. of SPIE*, 1997, 2988:257~263.

[10] Johnson B. Thermal-blooming laboratory experiments [J]. *The Lincoln Laboratory Journal*, 1992, 5 (1): 151~169.

[11] 孙运强. 激光内通道传输的气体热效应研究[D],长沙:国防科学技术大学,2011:42-43.

SUN Y Q.*Study on the Thermal Blooming of Beam Propagation in the inner channel*[D].Changsha: Graduate School of National University of Defense Technology,2011:42-43.(in Chinese)

[12] 朱福音.激光内通道热效应研究[D]，成都：中国科学院光电技术研究所，2017：6-16.

ZHU F Y.*Research on the Thermal blooming of Laser Propagation in the Inner Channel*[D].Cheng du:Institute of Optics and Electronics Chinese Academy of Sciences,2017:6-16.(in Chinese)

[13] 胡鹏，张建柱，张飞舟.高能激光系统内光路热效应建模与仿真[J].强激光与粒子束,2022，34(1):0110081-01100811.

HU P,ZHANG J Z,ZHANG F Z.Modeling and analysis of inner thermal effects in high energy laser system[J].*High Power Laser and Particle Beams*,2022，34(1):0110081-01100811.(in Chinese)

[14] Rui Zhou,Ding Cui,Xueting Liu,et al.Influence of convective heat transfer on thermal blooming effect in high-power laser emission systems[J].*International Journal of Heat and Mass Transfer*,2024,230:125777.

[15] Lu Lu, Zhiqiang Wang, Pengfei Zhang, *et al*.Thermal blooming induced phase change and its compensation of a Gaussian beam propagation in an absorbing medium[J].*Optics Letters*,2021,46(17):4304-4307;

[16] Ferziger J H, Peric M. *Computational Methods for Fluid Dynamics* [M].Berlin- Springer, 1996.

[17] 陶文铨. 数值传热学［M］. 西安：西安交通大学出版社，2001:240-245

TAO W Q.*Numerical Heat Transfer*[M].Xian:Xi'an Jiaotong University Press,2001:240-245.(in Chinese)

[18] Fuyin Zhu,Jihong Wang,Ge Ren,*etal*.Thermal blooming on laser propagation in an aspirating pipe[J].*SPIE*,2016,10;

[19] 张琪，胡启立，王红燕，等.高能激光热晕效应数值模拟方法的适用范围分析[J]，中国激光，2024,51（8）：0808003-1-0805003-9.

ZHANG Q,HU Q L,WANG H Y,*et al*.Analysis of applicable scope of numerical simulation method for thermal blooming of high-energy laser[J],*Chinese Journal of Lasers,*2024,51（8）：0808003-1-0805003-9.

[20] G.Bonsch and E.Potulski.Measurement of the refractive index of air and comparison with modified Edl'en's formulae[J].*Metrologia*,1998,35(133):133-139

[21] Niu K, Tian C. Zernike polynomials and their applications[J]. Journal of Optics, 2022, 24(12): 123001.

[22] 霍宏伟, 金奇, 刘洋, 等. 离轴反射式光学系统的设计与装调分析[J]. 激光与红外, 2017, 47(3): 363-366.

HUO H W,JIN Q,LIU Y,et al.Design and alignment analysis of off-axis reflective optical system[J].*Laser & Infrared,*2017, 47(3): 363-366.

[23] Keith B.Doyle,Victor L.Genberg,GregoryJ.Michels.Integreted Optomechanical Analysis(Second Edition)[M].*Washington:SPIE*,2012:56.

[24] 兰硕, 李新南, 徐晨. 激光合束光学系统气体热效应影响分析[J].中国光学,2018,11（1）：108-11

LAN S,LI X N,XU C.Influence of gas thermal effect on beam combination system[J].Chinese Optics, 2018,11（1）：108-114.

[25] 刘万生, 袁志军, 王汉斌, 等.封闭通道浮力对流下阵列光束热晕效应分析[J].光学学报，2022,42（1）：0114001.

LIU W S,YUAN Z J,WANG H B,*et al.*Thermal blooming effect of array beams under buoyancy convection in closed channel[J].Acta optica sinica,2022,42（1）：0114001.

作者简介：

Wu Dong-yu (1999－), male, born in Shuangyashan, Heilongjiang Province, master candidate. He received his bachelor's degree from Anhui Polytechnic University in 2022. His research mainly focuses on the environmental adaptability analysis of optical precision instruments
E-mail：wudongyu1111@163.com

Li Xiang (1986－), male, born in Changchun, Jilin Province. Ph.D, associate researcher, and master supervisor. He received his Ph.D. from the Changchun Institute of Optics, Fine Mechanics and Physics, Chinese Academy of Sciences in 2015. His research mainly focuses on laser propagation, optical system structure optimization design, analysis, and environmental adaptability research.
E-mail：abelfeel@163.com